BPR MCS | Bulletin of Pioneering Researches of Medical and Clinical Science

Bulletin of Pioneering Researches of Medical and Clinical Science

Available online: https://bprmcs.com
2025 | Volume 4 | Issue 2 | Page: 75-88

Investigating the Function and Therapeutic Potential of Melatonin-Regulated KLF6 in Intracranial Aneurysm Formation

Sangiliyandi Gurunathan[1]*, Min-Hee Kang[1], Jin-Hoi Kim[1]

[1] Department of Stem Cell and Regenerative Biotechnology, Konkuk University, Seoul 05029, Korea.

Abstract

Intracranial aneurysm (IA) is a life-threatening cerebrovascular condition, often fatal when complicated by subarachnoid hemorrhage. While Krüppel-like factor 6 (KLF6) has been implicated in cancer and cardiovascular pathologies, its role in IA remains largely unexplored. The present study aims to clarify KLF6's involvement in IA and identify potential therapeutic agents, advancing understanding and management of this condition. Gene expression datasets GSE122897 and GSE15629 were retrieved from the GEO database for analysis. The study examined the impact of KLF6 on IA through immune cell profiling and hypoxia-related pathways. Weighted gene co-expression network analysis (WGCNA) was applied to identify KLF6-associated hub genes. Hypoxia-related genes were further characterized, and computational drug screening was performed to pinpoint potential therapeutics. Blood samples from IA patients and healthy controls were evaluated for endothelin-1 (ET-1), vascular hematoma factor (vWF), and KLF6 expression. An in vitro model of H_2O_2-induced injury in human brain vascular smooth muscle cells (HBVSMCs) was employed to assess the effects of KLF6 modulation and melatonin treatment. Patients with elevated KLF6 expression showed significant alterations in resting memory $CD4^+$ T cells and monocyte populations. Gene set enrichment analyses revealed that four hypoxia-related pathways were strongly activated in the high KLF6 group. Six hub genes linked to hypoxia demonstrated robust correlations with KLF6 expression. Drug prediction analyses highlighted melatonin as a potential candidate for IA therapy. ET-1, vWF, and KLF6 levels were significantly increased in IA patients. In HBVSMCs, KLF6 intensified H_2O_2-induced cellular injury, an effect counteracted by melatonin treatment. KLF6 may serve as a novel therapeutic target in IA, and melatonin's modulation of KLF6-related pathways could offer protective effects against IA progression.

Keywords: Intracranial aneurysm, Melatonin, KLF6, Hypoxia, Immune microenvironment

Corresponding author: Sangiliyandi Gurunathan
E-mail: gsangiliyandi@yahoo.com

Received: 03 June 2025
Revised: 27 September 2025
Accepted: 01 October 2025

How to Cite This Article: Gurunathan S, Kang MH, Kim JH. Investigating the Function and Therapeutic Potential of Melatonin-Regulated KLF6 in Intracranial Aneurysm Formation. Bull Pioneer Res Med Clin Sci. 2025;4(2):75-88. https://doi.org/10.51847/GvAOB8IiQa

Introduction

Intracranial aneurysm (IA) is a frequent cerebrovascular condition characterized by the localized dilation of weakened arterial walls, affecting roughly 3.2% of the population [1]. While many aneurysms remain stable, rupture can result in aneurysmal subarachnoid hemorrhage (SAH), often leading to severe neurological impairment or death [2]. The underlying mechanisms of IA formation and progression remain poorly understood, making prevention and therapeutic intervention challenging.

IA pathogenesis involves a complex interplay of cellular and molecular events. Endothelial dysfunction, phenotypic shifts in vascular smooth muscle cells (VSMCs), apoptosis, inflammatory responses, hypoxia, and extracellular matrix (ECM) remodeling all contribute to aneurysm development [3, 4]. Hemodynamic forces promote infiltration of inflammatory cells, which trigger VSMC transformation and ECM alterations, driving vessel wall remodeling [5, 6]. In parallel, hypoxic conditions within the aneurysmal wall stimulate angiogenesis and further recruit immune cells [7]. These interconnected processes create a microenvironment that favors the initiation, growth, and rupture of IA. Exploring the intersection of hypoxia and immune signaling in IA could offer insights into novel therapeutic strategies.

Krüppel-like factor 6 (KLF6) is a transcription factor regulating cell proliferation, differentiation, and apoptosis [8]. Dysregulated KLF6 expression has been linked to diverse pathologies, including cancers, cardiovascular disorders, and inflammation-related diseases [9]. Notably, KLF6 can influence ECM remodeling by regulating matrix metalloproteinases (MMPs) [10] and modulate inflammatory and hypoxic responses through HIF1α regulation in macrophages [11]. Our prior work showed that silencing KLF6 reduced H_2O_2-induced damage in human brain vascular smooth muscle cells (HBVSMCs), suggesting its potential role in IA pathophysiology [12]. Despite these findings, the specific mechanisms by which KLF6 contributes to IA remain elusive. The present study aims to clarify KLF6's involvement in IA and identify potential therapeutic agents, advancing understanding and management of this condition.

Materials and Methods

Dataset acquisition and processing

Gene expression data were sourced from the Gene Expression Omnibus (GEO) database and analyzed using R (version 3.5.3, https://www.r-project.org/). The term "intracranial aneurysm" was used for the search. Studies with single-sample data or conducted at the cellular or animal model level were excluded. Two datasets were selected for analysis: GSE122897, which contained 16 controls, 21 unruptured, and 22 ruptured IA samples, served as the training set, while GSE15629, comprising 5 controls, 6 unruptured, and 8 ruptured IA samples, was used for validation. Probe identifiers were converted to gene symbols according to the respective GPL platforms, and for genes mapped to multiple probes, mean expression values were calculated.

Evaluation of KLF6 expression and diagnostic potential

KLF6 expression levels were compared between IA patients and healthy controls in both datasets, visualized with box plots. Receiver operating characteristic (ROC) curve analysis was conducted using the pROC package to assess KLF6's ability to discriminate IA samples from controls, with the area under the curve (AUC) used to quantify diagnostic performance. Additional analyses examined KLF6 expression across patient subgroups defined by clinical characteristics within the GSE122897 dataset.

Analysis of the microenvironment

IA samples from the GSE122897 dataset were divided into two groups according to KLF6 expression, using the median value as the cutoff. Variations in immune cell infiltration between the high- and low-KLF6 groups were assessed with the Wilcoxon rank-sum test, and immune composition was illustrated using stacked bar charts. To explore hypoxic states, four established hypoxia gene sets—MANALO HYPOXIA UP, MENSE HYPOXIA UP, HALLMARK HYPOXIA, and HARRIS HYPOXIA—were subjected to gene set enrichment analysis (GSEA).

Gene set variation analysis (GSVA)

Gene set variation analysis (GSVA) was conducted using the "GSVA" R package to evaluate functional differences between KLF6 expression groups. The KEGG gene set "c2.cp.kegg.v7.2.symbols" from MSigDB was used as a reference. Differential pathway activity was quantified with the "limma" package, with significance determined at FDR < 0.05.

Identification of differentially expressed genes (DEGs)

For GSE122897, probe-level expression values were consolidated by averaging multiple probes for the same gene, followed by log2 transformation [$\log_2$(data + 1)]. DEGs between high- and low-KLF6 groups were identified using the "limma" package, with thresholds of $|\log_2$ fold change$| > 1$ and FDR < 0.05. Volcano plots and heat maps were used to visualize patterns of gene dysregulation.

Construction of Co-expression Networks (WGCNA)

A weighted gene co-expression network was constructed with the "WGCNA" R package. Samples were initially clustered using average linkage to detect outliers, which were removed using a cut height of 70. To achieve scale-free topology, the soft-thresholding power was set at $\beta = 6$, targeting an R^2 of 0.90. Modules were defined to include a minimum of 150 genes. The adjacency matrix was transformed into a topological overlap matrix (TOM), and a dissimilarity measure (1-TOM) was calculated. Dynamic tree cutting was used to define gene modules, and closely related modules were merged at a 0.25 height threshold.

Associations between modules and KLF6 expression levels were examined to identify relevant hub modules.

Identification of Hub Genes and functional enrichment

Within each hub module, genes with module membership |MM| > 0.6 and gene significance |GS| > 0.4 were considered key hub genes. These hub genes overlapped with previously identified DEGs to refine the candidate gene list. Functional annotation of hub genes was performed using gene ontology (GO) analysis via the DAVID database (https://david.ncifcrf.gov/), with significance defined as $P < 0.01$.

Integration of Hypoxia-related Genes

Hypoxia-associated genes were retrieved from the MSigDB database and intersected with the hub genes to identify hypoxia-relevant candidates. Correlation analyses were performed to explore relationships between these genes and KLF6 expression.

Feature selection and predictive model development

To identify potential biomarkers for IA diagnosis, LASSO regression ("glmnet" R package) was first applied to select key genes from the hub gene set. Random forest analysis ("randomForest" R package) was then used to rank the importance of these features based on the average decrease in accuracy. The optimal number of predictive features was determined by sequentially adding genes with 10-fold cross-validation. Finally, random forest and support vector machine ("e1071" R package) models were built, and their diagnostic performance, along with that of individual signature genes, was assessed using ROC curve analysis.

Drug prediction

Differential expression analysis was conducted on hub genes comparing IA samples to controls. Potential therapeutic agents targeting these hub genes were subsequently identified using the DGIdb database (https://dgidb.org/).

Cell culture and treatment protocols

Human brain vascular smooth muscle cells (HBVSMCs; Cat. No. CM-H116) were obtained from Procell (Wuhan, China) and maintained in DMEM supplemented with 10% fetal bovine serum (FBS) at 37 °C in a humidified atmosphere containing 5% CO_2. Cells were trypsinized and seeded into 6-well plates at a density of 2×10^5 cells per well. Six experimental groups were established: Control, H_2O_2, H_2O_2 + Melatonin, H_2O_2 + pcDNA-NC, H_2O_2 + pcDNA-KLF6, and H_2O_2 + pcDNA-KLF6 + Melatonin. Except for the control group, all other groups were exposed to 100 μM H_2O_2 for 6 hours, while the control group received an equivalent volume of PBS. Transfections of pcDNA-KLF6 and pcDNA vectors were performed using Lipofectamine 3000 (Thermo Scientific, USA) according to the manufacturer's instructions. For the H_2O_2 + Melatonin and H_2O_2 + pcDNA-KLF6 + Melatonin groups, 100 μM melatonin was added for 6 hours in combination with the other treatments.

Quantitative Real-Time PCR (RT-qPCR)

Total RNA was extracted using TRIzon Reagent (cwbio, China) and reverse-transcribed into cDNA with the Evo M-MLV Reverse Transcription Kit (Accurate Biology, China). KLF6 expression was quantified by RT-qPCR using GAPDH as an internal control. Amplification was performed with SYBR Green Pro Taq HS Mix (Takara Bio, Japan) under the following conditions: initial denaturation at 95 °C for 30 s, followed by 40 cycles of 95 °C for 5 s and 60 °C for 30 s, repeated three times. Relative expression levels were calculated using the 2^–ΔΔCt method, and P-values < 0.05 were considered statistically significant. Primer sequences were as follows:
KLF6: forward 5′-GGCCAAGTTTACCTCCGACC-3′; reverse 5′-TAAGGCTTTTCTCCTTCCCTGG-3′
GAPDH: forward 5′-TTCTTTTGCGTCGCCAGGTG-3′; reverse 5′-GGAGGGAGAGAACAGTGAGC-3′

Cell proliferation assays

Cell proliferation was evaluated using MTT, colony formation, and EdU assays. For MTT, cells were seeded in 96-well plates at 6×10^3 cells per well and cultured for 24, 48, 72, and 96 hours. MTT solution (20 μL, 5 mg/mL; Sangon Biotech, China) was added for 4 hours, followed by medium removal and addition of 100 μL DMSO. Optical density was measured at 490–570 nm using a microplate reader (Thermo Fisher, USA).

For colony formation assays, cells were seeded in 6-well plates at 1×10^3 cells per well and cultured for 11 days, with medium replacement every 3 days. Colonies were fixed with 4% paraformaldehyde (1 mL) and stained with crystal violet (Sangon Biotech, China), then imaged under a fluorescence microscope (Olympus, Japan).

EdU incorporation assays were performed using the Click-iT EdU-488/555/647 Cell Proliferation Kit (Servicebio, China) following the manufacturer's instructions to assess DNA synthesis and proliferation activity.

Western blot analysis

Proteins were separated on 10% polyacrylamide gels and then transferred onto PVDF membranes. After blocking with 5 percent skim milk, membranes were incubated overnight at 4 °C with the following primary antibodies: KLF6 (1:800), GAPDH (1:50,000), Bax (1:20,000; Proteintech, USA), Bcl-2 (1:2,000), and cleaved caspase-3 (1:1,000; Abcam, UK). Membranes were subsequently treated with HRP-conjugated secondary antibodies (1:5,000; ZSGB-Bio, China), and protein bands were visualized using an ECL detection system (Servicebio).

Densitometric analysis of band intensities was performed using ImageJ software.

Flow cytometry for apoptosis

Cellular apoptosis was evaluated using the Annexin V-PE/7-AAD kit (Meilunebio, China) following the manufacturer's instructions. Three control conditions were included: untreated cells, cells stained only with 7-AAD, and cells stained only with Annexin V-PE. Data acquisition was performed with CellQuest software, generating two-dimensional dot plots with PE fluorescence on the x-axis and 7-AAD on the y-axis. Apoptotic cells were defined as the sum of Annexin V-PE^+/7-AAD^+ and Annexin V-PE^+ populations.

Patient samples

A total of 28 blood samples were collected, including 12 from healthy volunteers and 16 from patients with IA [12]. Expression of KLF6 at the mRNA and protein levels was assessed using RT-qPCR and western blotting, respectively. Serum levels of vascular hematoma factor (vWF) and endothelin-1 (ET-1) were measured using ELISA kits (Shanghai Fanke, China) according to the manufacturer's instructions. Ethical approval was obtained from the Medical Ethics Committee of Suzhou Hospital of Anhui Medical University (C2024002), and the study adhered to the Declaration of Helsinki. Written informed consent was obtained from all participants.

Statistical analysis

Comparisons of gene expression and immune cell infiltration between groups were conducted using the Wilcoxon rank-sum test. Associations between KLF6 expression and immune cell levels were determined using Pearson correlation coefficients. Data are expressed as mean ± standard deviation. For comparisons between two groups, independent sample t-tests were used, while one-way ANOVA was applied for comparisons among multiple groups. Statistical significance was defined as $P < 0.05$, and analyses were performed using SPSS version 22.0 software.

Results

KLF6 expression characteristics

KLF6 is located on chromosome 10 **(Figure 1A)**. Analysis of the GSE122897 and GSE15629 datasets revealed that KLF6 expression was markedly higher in IA samples than in controls, with AUC values of 0.701 and 0.829, respectively **(Figures 1B and 1C)**, indicating potential utility as a diagnostic biomarker. Further subgroup analysis within GSE122897 showed that KLF6 expression was not significantly influenced by aneurysm rupture status, patient age, or sex **(Figure 1D)**.

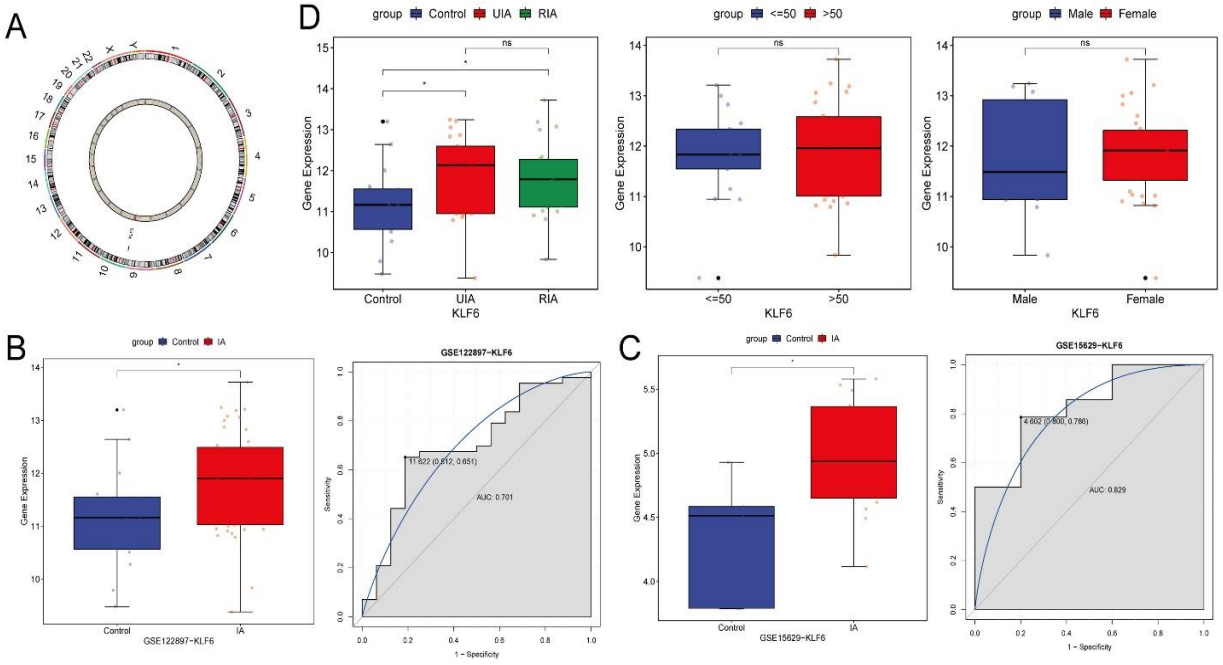

Figure 1. KLF6 expression characteristics: (A) Chromosomal location of KLF6, (B–C) KLF6 expression levels and corresponding ROC analyses in the GSE122897 and GSE15629 datasets, and (D) KLF6 expression across clinical subgroups, including ruptured versus unruptured aneurysms, age groups, and sex. UIA/RIA: unruptured/ruptured intracranial aneurysm

Microenvironmental Analysis and KLF6

Using the median KLF6 expression value in the GSE122897 dataset, IA samples were stratified into high-

and low-KLF6 expression groups, comprising 21 and 22 samples, respectively. Analysis of the immune microenvironment revealed significant differences in the levels of resting memory CD4⁺ T cells and monocytes between the two groups **(Figure 2A)**. Although the GSE15629 dataset did not reach statistical significance for these cell types, a consistent trend in the same direction was observed **(Figure 2B)**. Correlation analysis further demonstrated that KLF6 expression was positively associated with resting memory CD4⁺ T cells (r = 0.37) and negatively associated with monocytes (r = −0.46) **(Figure 2C)**.

To explore the connection between KLF6 and hypoxia, gene set enrichment analysis (GSEA) was performed on four hypoxia-related gene sets. All sets showed enrichment in the high-KLF6 group, with MANALO HYPOXIA UP and HALLMARK HYPOXIA reaching statistical significance ($P < 0.05$) **(Figure 2D)**. These results indicate that KLF6 may play a role in modulating both the immune microenvironment and hypoxic responses in intracranial aneurysms.

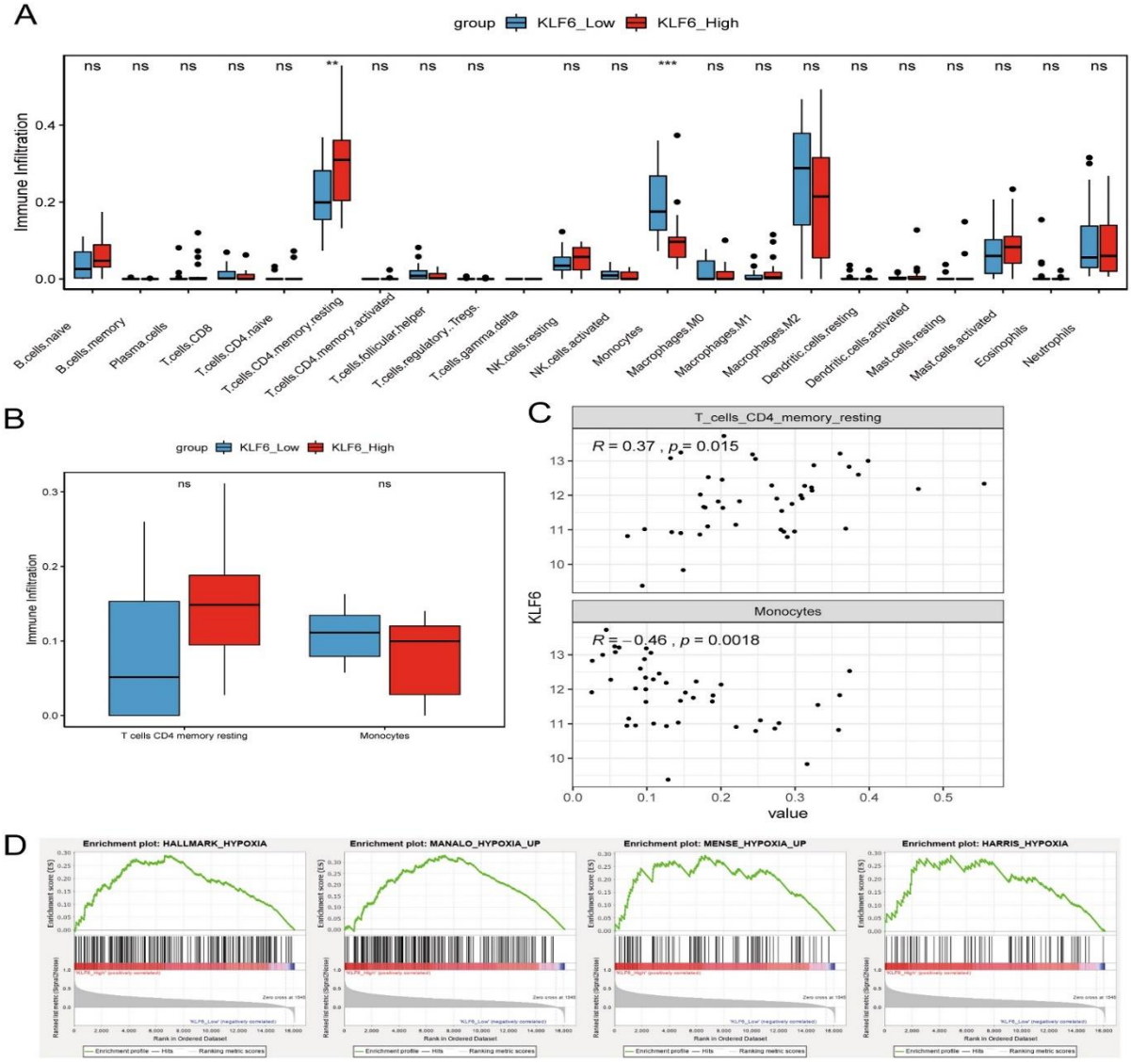

Figure 2. Analysis of the IA microenvironment: (A) Comparison of immune cell infiltration patterns in groups with high versus low KLF6 expression, (B) Assessment of T cells, CD4 memory resting, and monocyte infiltration within the GSE15629 dataset, (C) Relationship between KLF6 expression and the levels of T cells, CD4 memory resting, and monocytes, and (D) GSEA highlighting hypoxia-associated gene sets in the context of differing KLF6 expression levels

GSVA analysis

To determine how KLF6 expression affects biological processes in IA, we applied GSVA to compare high- and low-expression groups. The analysis revealed 18 pathways with differential activity. Specifically, six pathways were enriched in the low KLF6 group, including neuroactive ligand-receptor interaction, tryptophan and histidine metabolism, and retinol metabolism. In contrast, twelve pathways were more active when KLF6 expression was high, encompassing processes such as autophagy regulation, ubiquitin-mediated proteolysis, protein export, basal transcription factor function, and GPI-anchor biosynthesis **(Figure 3)**. These observations suggest that

KLF6 may play a central role in modulating diverse cellular and metabolic pathways in IA.

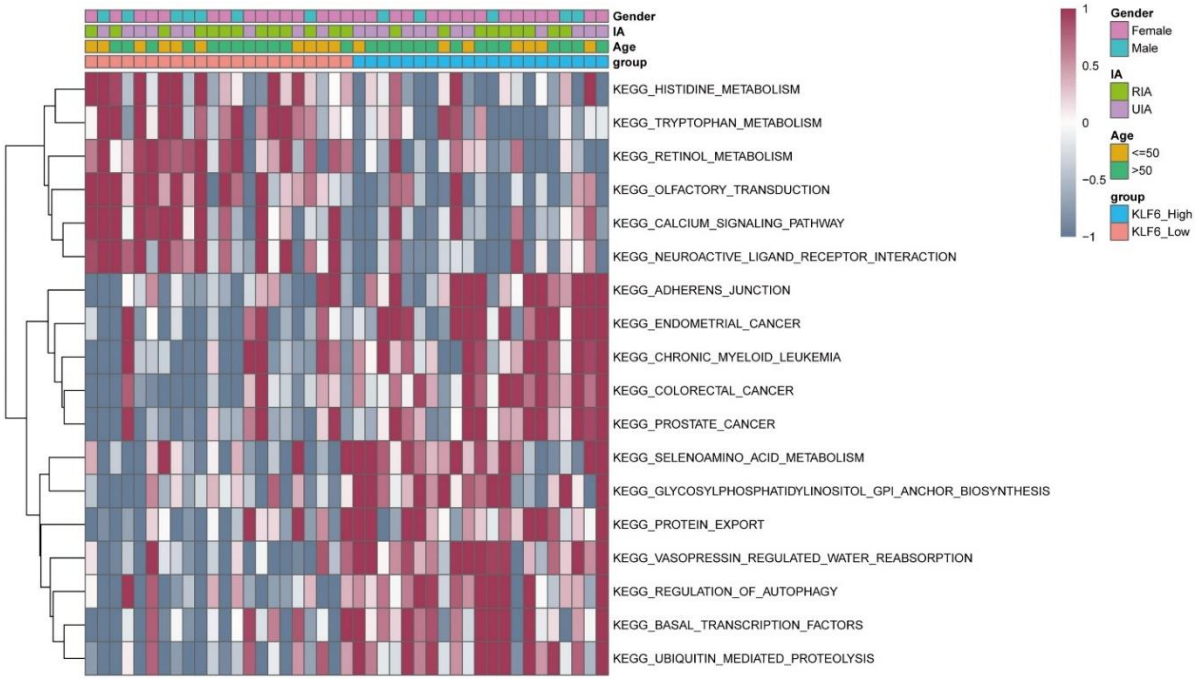

Figure 3. GSVA analysis. GSVA analysis in high and low KLF6 expression groups

Identification of DEGs and Hub Genes

In comparison to the low KLF6 expression group, the high KLF6 expression group exhibited 1,840 differentially expressed genes (DEGs), with 1,839 being upregulated and only one downregulated **(Figure 4A and 4B)**. Using WGCNA, sixteen candidate gene modules were initially identified **(Figure 4C)**. Of these, three modules—MEbrown (P = 0.04), MEyellow (P = 8e-04), and MEblack (P = 0.01)—showed significant associations with KLF6 expression levels and were designated as hub modules **(Figure 4D)**. Within these hub modules, 396 genes were found to correlate with high and low KLF6 expression **(Figure 4E)**. By intersecting these 396 genes with the identified DEGs, 76 hub genes were obtained. Enrichment analyses indicated that these hub genes predominantly localize to the nucleus and nucleoplasm and are likely crucial for transcriptional regulation. Functionally, they are implicated in processes such as circadian rhythm control, RNA polymerase II-mediated transcription, PDGF signaling, and broader cell signaling pathways **(Figure 4F)**.

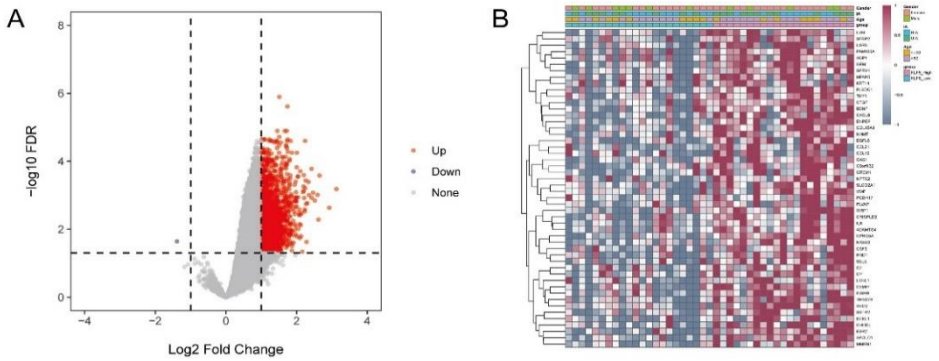

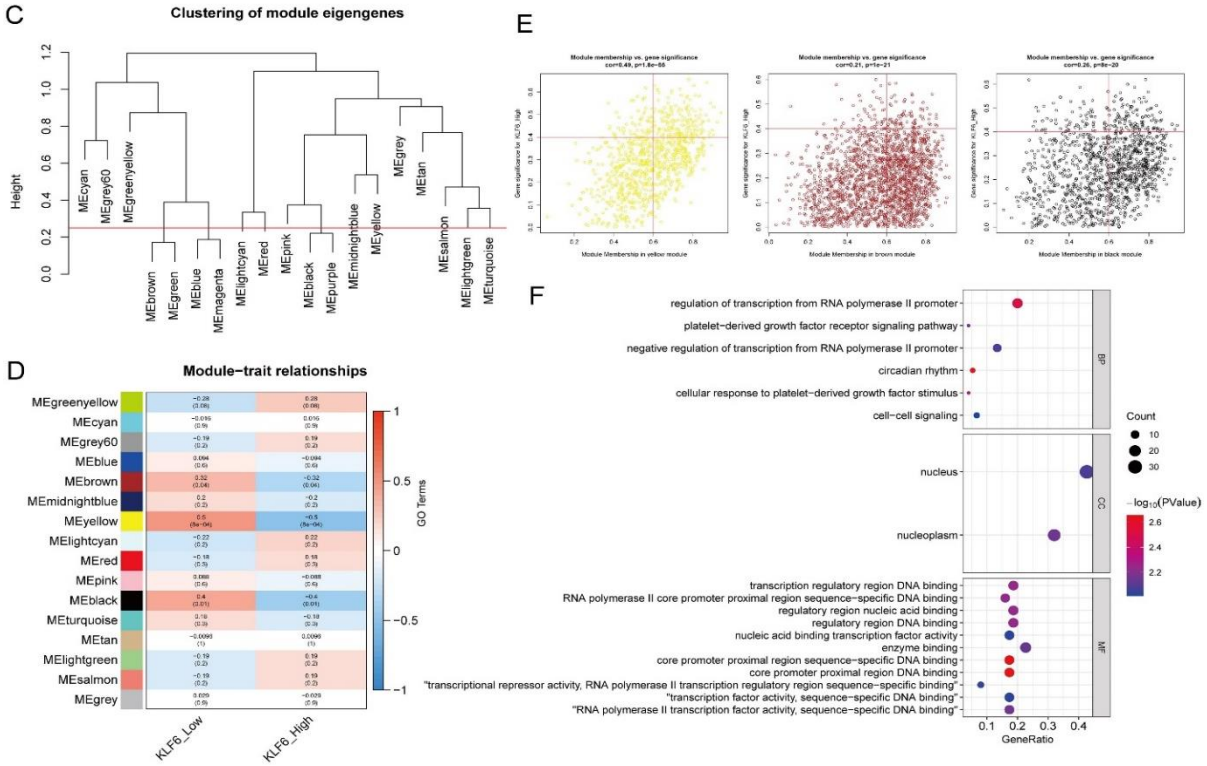

Figure 4. Identification of DEGs and hub genes. Differentially expressed genes (DEGs) were assessed between groups with high versus low KLF6 expression. These DEGs were visualized using (A) a volcano plot and (B) heatmaps. (C) Module eigengenes were subjected to clustering, and (D) their correlations with KLF6 expression were displayed in a heatmap. Modules MEyellow, MEbrown, and MEblack were chosen for subsequent analyses. (E) The relationship between module membership (MM, X-axis) and gene significance (GS, Y-axis) was illustrated through scatter plots for the three selected modules. (F) Gene Ontology (GO) analysis was conducted to explore the functional roles of hub genes

Hub genes and hypoxia

To examine the interplay between KLF6 and hypoxia, 200 hypoxia-associated genes were extracted from the MSigDB database. These were intersected with hub genes, revealing six hypoxia-related hub genes: KLF6, ERRFI1, ETS1, MAFF, NFIL3, and TIPARP **(Figure 5A)**. Of these, KLF6 and NFIL3 were significantly overexpressed in IA samples compared to controls, while ERRFI1, MAFF, and TIPARP showed an upward expression trend (Figure 5B). Furthermore, ERRFI1, ETS1, MAFF, NFIL3, and TIPARP were markedly upregulated in the high KLF6 group and demonstrated positive correlations with KLF6 expression, with TIPARP showing the strongest association (r = 0.81) **(Figures 5C and 5D)**.

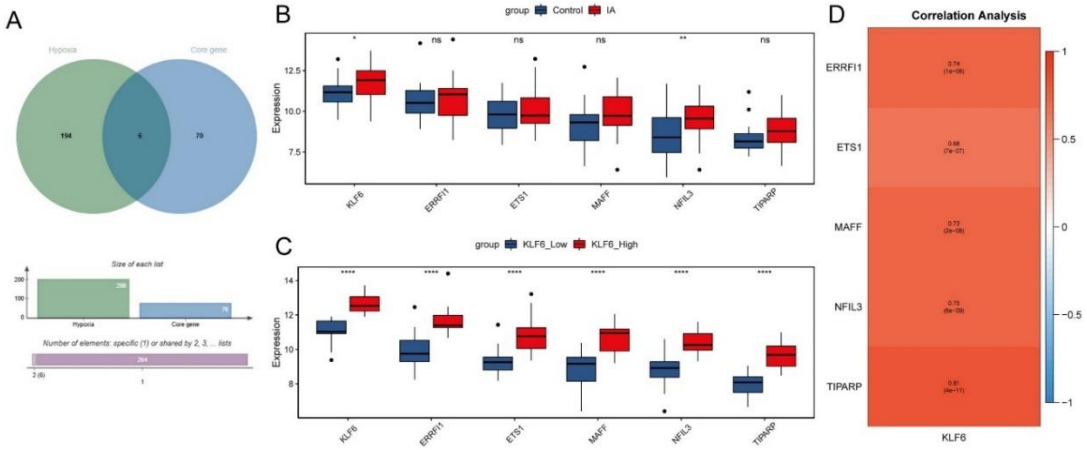

Figure 5. Hypoxia analysis: (A) Overlap of hypoxia-related genes with hub genes identified the subset of hypoxia-associated hub genes, (B) Expression profiles of these hypoxia-related hub genes were compared between IA and control samples, (C) Expression levels of the same genes were assessed between groups with high and low KLF6 expression, and (D) Correlation analysis was performed to examine the relationship between KLF6 and the hypoxia-related hub genes

Identification of signature genes and model construction

From the 76 hub genes, LASSO analysis pinpointed eight candidate genes, which were ranked according to mean decrease in accuracy **(Figure 6A)**. Ten-fold cross-validation indicated that the optimal predictive performance was achieved with four genes **(Figure 6B)**. Consequently, NPTX1, PTP4A1, NEDD8, and DUSP1 were selected as signature genes. Correlation analysis revealed strong associations between KLF6 and NEDD9, PTP4A1, and DUSP16 **(Figure 6C)**. Using these four signature genes, classification models were developed, with ROC analysis yielding AUCs of 0.834 for the SVM model and 0.791 for the RF model **(Figure 6D)**. Notably, these models outperformed the predictive power of any single signature gene, underscoring the advantage of their combined use **(Figure 6E)**. Additionally, NEDD9, NPTX1, and PTP4A1 showed significantly different expression between IA and control samples **(Figure 6F)**, with these findings further confirmed in the independent GSE15629 dataset **(Figure S1)**.

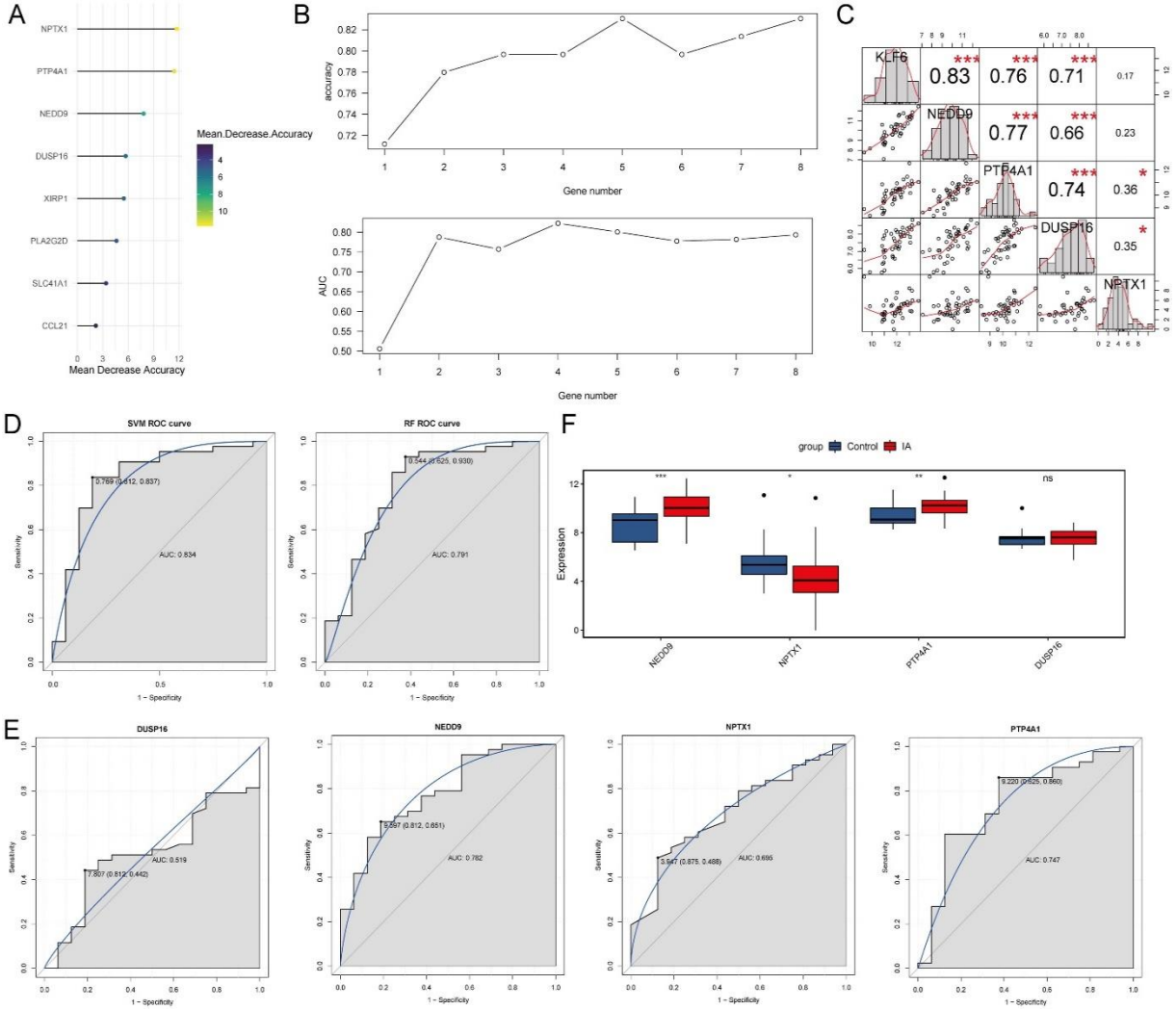

Figure 6. Identification of signature genes and development of diagnostic models: (A) LASSO analysis screened eight candidate genes, ranked according to mean decrease in accuracy, (B) Ten-fold cross-validation determined the optimal number of genes, resulting in the selection of NPTX1, PTP4A1, NEDD9, and DUSP16 as signature genes for further study, (C) Correlation analysis was performed between KLF6 and the signature genes, (D) ROC analysis was conducted for the SVM and RF models, (E) ROC curves for each signature gene were also assessed, and (F) Expression levels of the signature genes were compared between IA and control samples

Drug prediction

Differential expression analysis of the 76 hub genes identified 22 genes showing significant differences between IA and control samples **(Figure 7A)**. Of these 22, seven hub genes were linked to potential drug interactions according to the DGIdb database. Among them, MYC was associated with the most significant number of drugs, including melatonin **(Figure 7B)**.

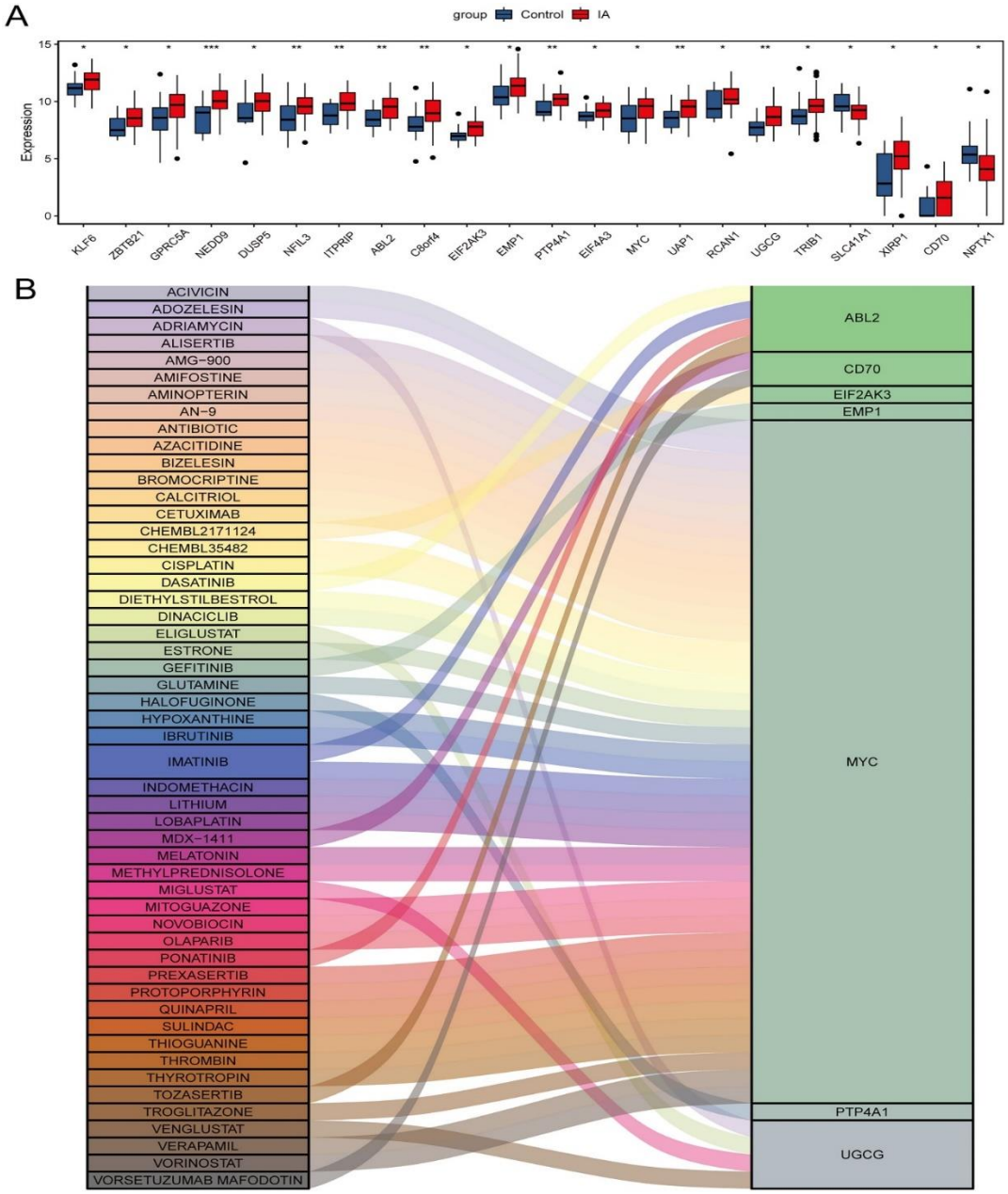

Figure 7. Drug prediction: (A) Differential expression analysis of hub genes in IA and control samples, and (B) Drug-gene interactions in the DGIdb database

KLF6 expression was elevated in individuals with IA

Endothelin-1 (ET-1) and von Willebrand factor (vWF), both markers commonly linked to vascular injury and inflammation, were found at significantly higher levels in IA patients **(Figures 8A and 8B)**. Additionally, both mRNA and protein expression of KLF6 were markedly increased in these patients **(Figures 8C and 8D)**.

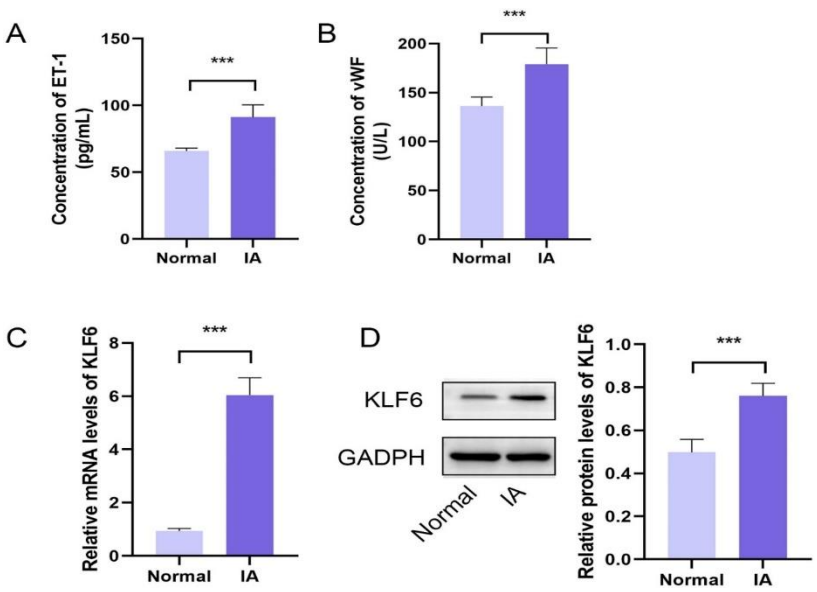

Figure 8. Serum and blood levels of ET-1, vWF, and KLF6 in IA. (A) Serum ET-1 and (B) vWF concentrations were measured using ELISA. (C) KLF6 mRNA levels and (D) protein expression in blood were assessed via RT-qPCR and Western blot, respectively. *P < 0.05, **P < 0.01, ***P < 0.001

Overexpression of KLF6 aggravates H_2O_2-induced HBVSMC injury

To mimic IA progression, an H_2O_2-induced HBVSMC injury model was established. KLF6 expression was significantly elevated in HBVSMCs treated with H_2O_2 compared to controls **(Figure 9A and 9B)**. Given the upregulation of KLF6 in IA patients, we hypothesized that KLF6 might contribute to IA development. To test this, HBVSMCs were transfected with a KLF6 overexpression vector before H_2O_2 exposure. MTT assays revealed that H_2O_2 treatment reduced cell proliferation, and KLF6 overexpression further suppressed proliferation **(Figure 9C)**. These results were corroborated by plate cloning and EDU assays, which showed similar reductions in cell growth **(Figure 9D and 9E)**. Western blot analysis indicated that pro-apoptotic proteins Bax and cleaved caspase-3 were significantly increased, while the anti-apoptotic protein Bcl-2 was decreased in the H_2O_2 model, demonstrating enhanced apoptosis **(Figure 9F)**. Overexpression of KLF6 further intensified apoptotic responses, as confirmed by flow cytometry **(Figure 9G)**. Collectively, these findings suggest that KLF6 overexpression exacerbates H_2O_2-induced injury in HBVSMCs.

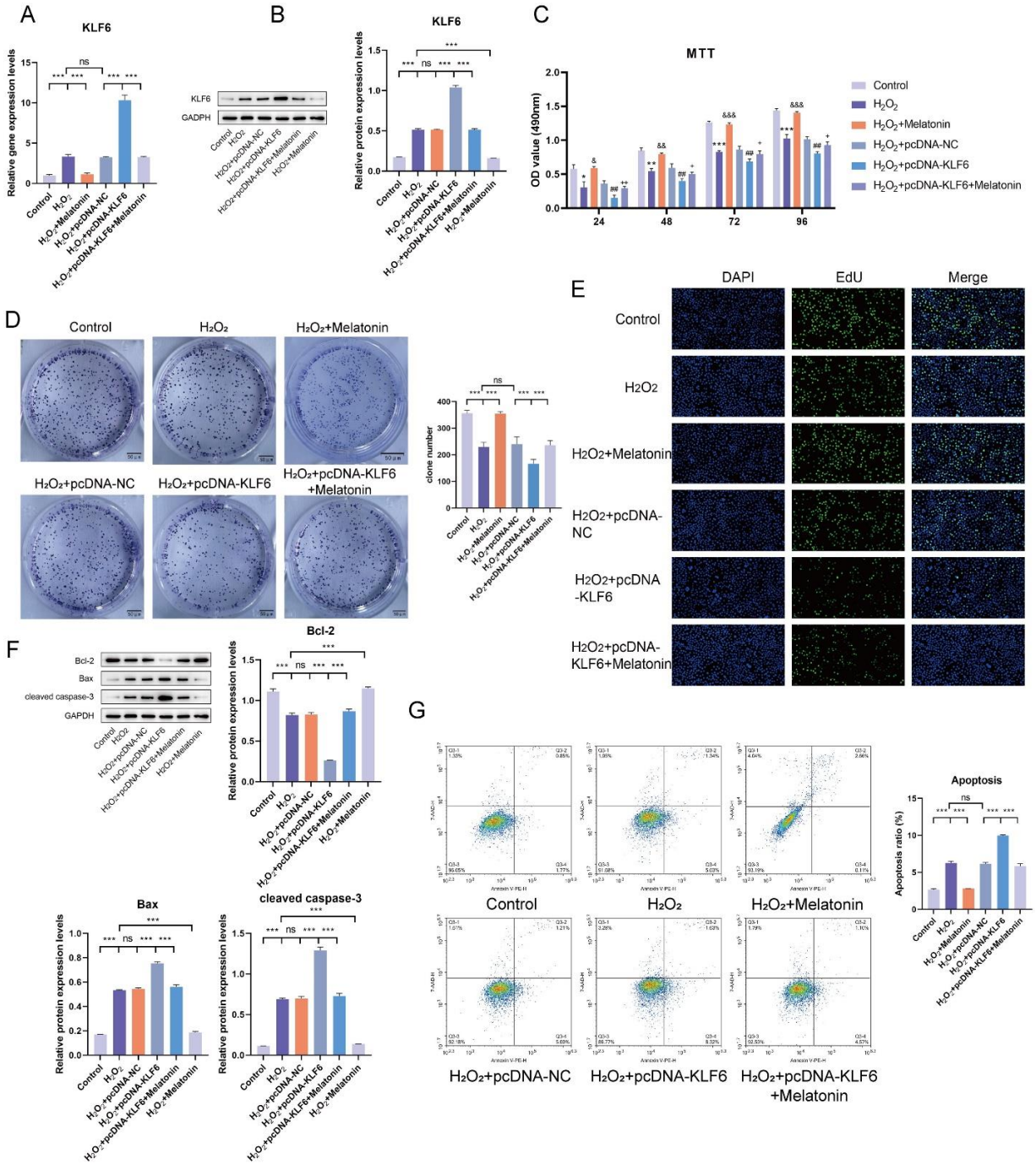

Figure 9. Melatonin mitigates KLF6-mediated exacerbation of H_2O_2-induced HBVSMC injury. (A) KLF6 mRNA and (B) protein levels were measured using RT-qPCR and Western blot, respectively. (C–E) MTT, plate cloning, and EDU assays were used to assess HBVSMC proliferation. * vs. H_2O_2, & vs. H_2O_2, # vs. H_2O_2+pcDNA-NC, + vs. H_2O_2+pcDNA-KLF6+melatonin. (F) Protein expression of apoptosis-related factors, including Bcl-2, Bax, and cleaved caspase-3, was evaluated. (G) Flow cytometry was performed to quantify HBVSMC apoptosis. ***P < 0.001

Melatonin attenuates H_2O_2-induced HBVSMC injury by regulating KLF6

The role of melatonin in the H_2O_2-induced HBVSMC injury model was further examined. Treatment with melatonin reduced KLF6 expression in the injured cells **(Figure 9A and 9B)**. Compared with the H_2O_2 group, melatonin treatment enhanced cell proliferation and decreased apoptosis, indicating a partial restoration toward baseline levels **(Figure 9C–9G)**. Furthermore, in cells overexpressing KLF6 (H_2O_2+pcDNA-KLF6), melatonin alleviated the KLF6-mediated worsening of injury by promoting proliferation and reducing apoptosis **(Figure 9C–9G)**. Collectively, these findings suggest that melatonin can mitigate H_2O_2-induced HBVSMC injury through modulation of KLF6.

Discussion

Intracranial aneurysms (IAs), also referred to as cerebral aneurysms, are relatively prevalent and carry a high risk of mortality if rupture occurs. Notably, approximately 12% of patients with SAH caused by ruptured IA experience immediate death [13]. Despite extensive research, the underlying mechanisms driving IA formation, progression, and rupture remain poorly understood. Emerging evidence suggests that hypoxia and the immune microenvironment play a role in IA pathogenesis [14]. In this study, we systematically investigated the involvement of KLF6 in IA, its interactions with hypoxia and immune processes, and identified potential therapeutic targets.

KLF6, a member of the Sp1/KLF transcription factor family, regulates gene expression, and its dysregulation has been linked to various diseases [15, 16]. Our results demonstrated that KLF6 expression was significantly elevated in IA samples compared to controls. ROC analysis further indicated the diagnostic potential of KLF6 in IA. Functional enrichment (GO) analysis revealed that 76 hub genes were involved in transcriptional regulation, cell signaling, and PDGF signaling pathways. Previous studies have highlighted the importance of these pathways in maintaining vascular wall integrity, suggesting that disruptions may contribute to IA development and progression [17–20]. Taken together, our findings support a pivotal role for KLF6 in IA pathogenesis and suggest its potential as a biomarker for the disease.

A central aspect of IA pathophysiology is the interplay between KLF6 and immune cell dynamics. Hemodynamic stress contributes to the development of IA by triggering excessive inflammatory and immune responses within the vessel wall [21]. Immune cell infiltration is a key contributor to IA progression [22]. Our findings suggest that KLF6 may regulate the infiltration of resting memory $CD4^+$ T cells and monocytes, which are known to be dysregulated in IA patients [23] and play a role in the inflammatory environment of the disease [24, 25]. Previous research has demonstrated that KLF6 participates in endothelial dysfunction and modulates macrophage-driven inflammation [26, 27], further linking KLF6 to immune regulation in IA.

Hypoxia is another critical factor in IA pathogenesis. KLF6 expression is markedly upregulated in ischemia-reperfusion injury, a condition closely associated with hypoxia, and is linked to inflammation and apoptosis following injury [28]. In our study, GSEA revealed enrichment of hypoxia-related gene sets in the group with high KLF6 expression. Moreover, six hypoxia-related hub genes strongly associated with KLF6 were identified, which may influence IA rupture [29] or angiogenesis in cancer [30, 31], supporting the notion that KLF6 may modulate the hypoxic microenvironment in IA.

The four-gene signature model (NPTX1, PTP4A1, NEDD8, and DUSP16) demonstrated strong diagnostic performance and could facilitate precision medicine approaches for IA, enabling more tailored treatment strategies. These genes are involved in neural-related angiogenesis [32], signal transduction [33], protein ubiquitination [34], and cell cycle regulation [35], which aligns with the GSVA results observed across high and low KLF6 expression groups.

Vascular smooth muscle cells (VSMCs) are central to IA pathogenesis [36]. Oxidative stress-induced inflammation drives VSMC phenotypic changes, extracellular matrix dysregulation, and apoptosis, which collectively increase the risk of arterial wall thinning and rupture [37, 38]. KLF6 translocation promotes IL-6 release from VSMCs and participates in vascular injury and remodeling [39]. Additionally, KLF6 is closely linked to TGF-β signaling in endothelial remodeling [40]. Our results demonstrated that KLF6 overexpression aggravated H_2O_2-induced HBVSMC injury, highlighting KLF6 as a potential therapeutic target in IA.

Melatonin, known for its antioxidant and anti-inflammatory properties [41], has been shown to inhibit NF-κB signaling and reduce MMP activity, suggesting potential therapeutic benefit in aneurysm models [42]. It also mitigates SAH-associated inflammation, and elevated serum melatonin levels have been associated with poor prognosis in SAH patients [43, 44]. Melatonin modulates pro-inflammatory cytokines and immune cell activity [45], and is linked to hypoxia regulation, potentially ameliorating hypoxia-induced injury [46]. In our study, melatonin attenuated KLF6-mediated exacerbation of H_2O_2-induced HBVSMC injury, supporting its potential as a therapeutic agent for IA.

This study has several limitations. First, due to patient heterogeneity, larger cohorts and alternative analytical approaches are needed to validate the robustness of our findings. Second, the roles of KLF6 in hypoxia and immune regulation were primarily inferred from bioinformatics analyses and require further experimental verification. Finally, although melatonin demonstrated protective effects in vitro, additional studies are necessary to confirm its safety and efficacy in clinical settings, which will provide valuable guidance for potential therapeutic strategies.

In summary, KLF6 appears to play a pivotal role in the onset and progression of IA by modulating hypoxia and the immune microenvironment. Furthermore, targeting KLF6, potentially through melatonin-mediated mechanisms, may offer promising therapeutic opportunities. These findings provide important insights into the pathogenesis, diagnosis, and treatment of IA.

Acknowledgments: None.

Conflict of interest: None.

Financial support: None.

Ethics statement: None.

References

1. Tawk RG, Hasan TF, D'Souza CE, Peel JB, Freeman WD. Diagnosis and treatment of unruptured intracranial aneurysms and aneurysmal subarachnoid hemorrhage. Mayo Clin Proc. 2021;96(7):1970–2000.
2. Liu HJ, Zhou H, Lu DL, Zhang JH, Guo F, Li J, et al. Intracranial mirror aneurysm: epidemiology, rupture risk, new imaging, controversies, and treatment strategies. World Neurosurg. 2019;127:165–75.
3. Etminan N, Dörfler A, Steinmetz H. Unruptured intracranial aneurysms: pathogenesis and individualized management. Dtsch Arztebl Int. 2020;117(14):235–42.
4. Etminan N, Rinkel GJ. Unruptured intracranial aneurysms: development, rupture and preventive management. Nat Rev Neurol. 2016;12(12):699–713.
5. Sheinberg DL, McCarthy DJ, Elwardany O, Luther EM, McCulloch T, Cawley CM, et al. Endothelial dysfunction in cerebral aneurysms. Neurosurg Focus. 2019;47(1):E3.
6. Wang Z, Ma J, Yue H, Sun L, Liu Y, Li Y, et al. Vascular smooth muscle cells in intracranial aneurysms. Microvasc Res. 2023;149:104554.
7. Ono I, Kayahara T, Kawashima A, Yoshida Y, Inoue M, Nakano H, et al. Hypoxic microenvironment as a crucial factor triggering events leading to rupture of intracranial aneurysm. Sci Rep. 2023;13(1):5545.
8. McConnell BB, Yang VW. Mammalian Krüppel-like factors in health and diseases. Physiol Rev. 2010;90(4):1337–81.
9. Syafruddin SE, Mohtar MA, Wan Mohamad Nazarie WF, Low TY. Two sides of the same coin: the roles of KLF6 in physiology and pathophysiology. Biomolecules. 2020;10(10):1378.
10. Lin Y, Wen-Jie Z, Chang-Qing L, Chen W, Zhang M, Liu Y, et al. Mir-22-3p/KLF6/MMP14 axis in fibro-adipogenic progenitors regulates fatty infiltration in muscle degeneration. FASEB J. 2020;34(9):12691–701.
11. Kim GD, Ng HP, Chan ER, Mahabeleshwar GH. Krüppel-like factor 6 promotes macrophage inflammatory and hypoxia response. FASEB J. 2020;34(2):3209–23.
12. Yue PD, Lu YN, Zhang L, Li H, Wang C, Wu Y, et al. Circ_FOXO3 regulates KLF6 through sponge adsorption of miR-122-5p to repress H2O2-induced HBVSMC proliferation, thus promoting IA development in vitro model. Acta Biochim Pol. 2022;69(4):767–72.
13. Pontes FGB, da Silva EM, Baptista-Silva JC, Yasuda MAS, Atallah ÁN. Treatments for unruptured intracranial aneurysms. Cochrane Database Syst Rev. 2021;5(5):CD013312.
14. Jin J, Duan J, Du L, Li Y, Xu Z, Wu H, et al. Inflammation and immune cell abnormalities in intracranial aneurysm subarachnoid hemorrhage: relevant signaling pathways and therapeutic strategies. Front Immunol. 2022;13:1027756.
15. Limame R, Op de Beeck K, Lardon F, De Wever O, Van Laere S, Pauwels P, et al. Krüppel-like factors in cancer progression: three fingers on the steering wheel. Oncotarget. 2014;5(1):29–48.
16. Huang Z, He H, Qiu F, Zhang J, Wang C, Zhang J, et al. Expression and prognosis value of the KLF family members in colorectal cancer. J Oncol. 2022;2022:6571272.
17. Sudar-Milovanovic E, Gluvic Z, Obradovic M, Zafirovic S, Radak D, Isenovic ER. Tryptophan metabolism in atherosclerosis and diabetes. Curr Med Chem. 2022;29(1):99–113.
18. Zhang J, Jin J, Yang W. Autophagy regulates the function of vascular smooth muscle cells in the formation and rupture of intracranial aneurysms. Zhejiang Da Xue Xue Bao Yi Xue Ban. 2019;48(5):552–9.
19. Schimmel L, Gordon E. The precise molecular signals that control endothelial cell-cell adhesion within the vessel wall. Biochem Soc Trans. 2018;46(6):1673–80.
20. Frösen J, Piippo A, Paetau A, Kangasniemi M, Niemelä M, Hernesniemi J, et al. Growth factor receptor expression and remodeling of saccular cerebral artery aneurysm walls: implications for biological therapy preventing rupture. Neurosurgery. 2006;58(3):534–41.
21. Soldozy S, Norat P, Elsarrag M, Chatrath A, Costello JS, Sokolowski JD, et al. The biophysical role of hemodynamics in the pathogenesis of cerebral aneurysm formation and rupture. Neurosurg Focus. 2019;47(1):E11.
22. Chalouhi N, Ali MS, Jabbour PM, Tjoumakaris SI, Gonzalez LF, Rosenwasser RH, et al. Biology of intracranial aneurysms: role of inflammation. J Cereb Blood Flow Metab. 2012;32(9):1659–76.
23. Ge P, Liu C, Chan L, Li Y, Du X, Zhou J, et al. High-dimensional immune profiling by mass cytometry revealed the circulating immune cell landscape in patients with intracranial aneurysm. Front Immunol. 2022;13:922000.
24. Zhang HF, Zhao MG, Liang GB, Liu Y, Zhang X, Wang H, et al. Dysregulation of CD4(+) T cell

subsets in intracranial aneurysm. DNA Cell Biol. 2016;35(2):96–103.
25. Wang J, Cao Y. Characteristics of circulating monocytes at baseline and after activation in patients with intracranial aneurysm. Hum Immunol. 2020;81(1):41–7.
26. Wei G, Zhu D, Sun Y, Xu J, Li C, Zhang H, et al. The protective effects of azilsartan against oscillatory shear stress-induced endothelial dysfunction and inflammation are mediated by KLF6. J Biochem Mol Toxicol. 2021;35(6):e22737.
27. Kim GD, Ng HP, Patel N, Mahabeleshwar GH. Krüppel-like factor 6 and miR-223 signaling axis regulates macrophage-mediated inflammation. FASEB J. 2019;33(10):10902–15.
28. Li J, Yu D, He C, Guo W, Xie H, Chen J, et al. KLF6 alleviates hepatic ischemia-reperfusion injury by inhibiting autophagy. Cell Death Dis. 2023;14(7):393.
29. Aoki T, Kataoka H, Nishimura M, Ishibashi R, Nozaki K, Hashimoto N. Ets-1 promotes the progression of cerebral aneurysm by inducing the expression of MCP-1 in vascular smooth muscle cells. Gene Ther. 2010;17(9):1117–23.
30. Wang M, Zhao Y, Yu ZY, Ding Y, Li N, Yang L, et al. Glioma exosomal microRNA-148a-3p promotes tumor angiogenesis through activating the EGFR/MAPK signaling pathway via inhibiting ERRFI1. Cancer Cell Int. 2020;20(1):518.
31. Miura K, Koyanagi-Aoi M, Maniwa Y, Nishikawa Y, Aoi T. Chorioallantoic membrane assay revealed the role of TIPARP in lung adenocarcinoma-induced angiogenesis. Cancer Cell Int. 2023;23(1):34.
32. Li H, Yan R, Chen W, Wang Q, Wang C, Zhang Z, et al. Long non coding RNA SLC26A4-AS1 exerts antiangiogenic effects in human glioma by upregulating NPTX1 via NFKB1 transcriptional factor. FEBS J. 2021;288(1):212–28.
33. Campbell AM, Zhang ZY. Phosphatase of regenerating liver: a novel target for cancer therapy. Expert Opin Ther Targets. 2014;18(5):555–69.
34. Baek K, Krist DT, Prabu JR, Hill S, Klügel M, Neumaier LM, et al. NEDD8 nucleates a multivalent cullin-RING-UBE2D ubiquitin ligation assembly. Nature. 2020;578(7795):461–6.
35. Zhang H, Zheng H, Mu W, He Z, Yang B, Yang F, et al. DUSP16 ablation arrests the cell cycle and induces cellular senescence. FEBS J. 2015;282(23):4580–94.
36. Rahmani R, Baranoski JF, Albuquerque FC, Nakaji P, Newman CB, Bendok BR. Intracranial aneurysm calcification: a narrative review. Exp Neurol. 2022;353:114052.
37. Starke RM, Chalouhi N, Ali MS, Jabbour PM, Tjoumakaris SI, Gonzalez LF, et al. The role of oxidative stress in cerebral aneurysm formation and rupture. Curr Neurovasc Res. 2013;10(3):247–55.
38. Texakalidis P, Sweid A, Mouchtouris N, Peterson EC, Sioka C, Rangel-Castilla L, et al. Aneurysm formation, growth, and rupture: the biology and physics of cerebral aneurysms. World Neurosurg. 2019;130:277–84.
39. Garrido-Martín EM, Blanco FJ, Roquè M, Novoa JM, Tarín C, Pietras A, et al. Vascular injury triggers Krüppel-like factor 6 mobilization and cooperation with specificity protein 1 to promote endothelial activation through upregulation of the activin receptor-like kinase 1 gene. Circ Res. 2013;112(1):113–27.
40. Botella LM, Sanz-Rodriguez F, Komi Y, Fernandez-L A, Varela E, Garrido-Martin EM, et al. TGF-beta regulates the expression of transcription factor KLF6 and its splice variants and promotes co-operative transactivation of common target genes through a Smad3-Sp1-KLF6 interaction. Biochem J. 2009;419(2):485–95.
41. Ahmad SB, Ali A, Bilal M, Younis S, Rehman A, Shahid N, et al. Melatonin and health: insights of melatonin action, biological functions, and associated disorders. Cell Mol Neurobiol. 2023;43(6):2437–58.
42. Tang L, Cong Z, Hao S, Wu Y, Jiang Z, Li L, et al. Protective effect of melatonin on the development of abdominal aortic aneurysm in a rat model. J Surg Res. 2017;209:266–72.
43. Zhan CP, Zhuge CJ, Yan XJ, Xu J, Feng Y, Li Y, et al. Measuring serum melatonin concentrations to predict clinical outcome after aneurysmal subarachnoid hemorrhage. Clin Chim Acta. 2021;513:1–5.
44. Ahmed H, Khan MA, Kahlert UD, Fadul CE, Ding D, Sheen JJ, et al. Role of adaptor protein myeloid differentiation 88 (MyD88) in post-subarachnoid hemorrhage inflammation: a systematic review. Int J Mol Sci. 2021;22(8):4185.
45. Hardeland R. Aging, melatonin, and the pro- and anti-inflammatory networks. Int J Mol Sci. 2019;20(5):1223.
46. Bastani S, Akbarzadeh M, Rastgar Rezaei Y, Ahmadi A, Jalili A, Khosravi M, et al. Melatonin as a therapeutic agent for the inhibition of hypoxia-induced tumor progression: a description of possible mechanisms involved. Int J Mol Sci. 2021;22(19):10874.